AGU PUBLICATIONS

JGR

Journal of Geophysical Research: Space Physics

RESEARCH ARTICLE
10.1002/2017JA024902

Key Points:
- Superposed EPOCH analysis of relativistic electron enhancement and persistent depletion events at GEO to characterize solar wind parameters
- Differences between enhancement and persistent depletion events allow to establish a set of threshold values to characterize the events
- Using the threshold values for solar wind parameters, we test a simple method for predictability of relativistic electron enhancement events

Supporting Information:
- Supporting Information S1

Correspondence to:
V. A. Pinto,
vpinto@ucla.edu

Citation:
Pinto, V. A., Kim, H.-J., Lyons, L. R., & Bortnik, J. (2018). Interplanetary parameters leading to relativistic electron enhancement and persistent depletion events at geosynchronous orbit and potential for prediction, *Journal of Geophysical Research: Space Physics*, *123*. https://doi.org/10.1002/2017JA024902

Received 18 OCT 2017
Accepted 9 JAN 2018
Accepted article online 11 JAN 2018

Interplanetary Parameters Leading to Relativistic Electron Enhancement and Persistent Depletion Events at Geosynchronous Orbit and Potential for Prediction

Victor A. Pinto[1], **Hee-Jeong Kim**[1], **Larry R. Lyons**[1], **and Jacob Bortnik**[1]

[1]Department of Atmospheric and Oceanic Sciences, University of California, Los Angeles, CA, USA

Abstract We have identified 61 relativistic electron enhancement events and 21 relativistic electron persistent depletion events during 1996 to 2006 from the Geostationary Operational Environmental Satellite (GOES) 8 and 10 using data from the Energetic Particle Sensor (EPS) >2 MeV fluxes. We then performed a superposed epoch time analysis of the events to find the characteristic solar wind parameters that determine the occurrence of such events, using the OMNI database. We found that there are clear differences between the enhancement events and the persistent depletion events, and we used these to establish a set of threshold values in solar wind speed, proton density and interplanetary magnetic field (IMF) B_z that can potentially be useful to predict sudden increases in flux. Persistent depletion events are characterized by a low solar wind speed, a sudden increase in proton density that remains elevated for a few days, and a northward turning of IMF B_z shortly after the depletion starts. We have also found that all relativistic electron enhancement or persistent depletion events occur when some geomagnetic disturbance is present, either a coronal mass ejection or a corotational interaction region; however, the storm index, *SYM-H*, does not show a strong connection with relativistic electron enhancement events or persistent depletion events. We have tested a simple threshold method for predictability of relativistic electron enhancement events using data from GOES 11 for the years 2007–2010 and found that around 90% of large increases in electron fluxes can be identified with this method.

1. Introduction

The fluxes of relativistic electron populations in the Earth's outer radiation belt are highly variable. There is a long-term variability that has been suggested to be modulated by the solar cycle (Baker et al., 1986), but large variations also occur on short time scales. For example, sudden drops in flux levels that are typically followed by quick recoveries can occur on time scales of hours or days. Numerous studies have linked the short- and long-term variations of relativistic electron flux levels to different solar wind and magnetospheric parameters; the solar wind velocity (Baker et al., 1998; Blake et al., 1997; Lyons et al., 2005, 2009; Paulikas & Blake, 1979; Reeves et al., 2011; Wing et al., 2016), showing that high-speed streams are favorable for increases in flux, the change and orientation of the interplanetary magnetic field B_z (Blake et al., 1997; Boynton et al., 2016; Gao et al., 2015; Iles et al., 2002; Li et al., 2005; Miyoshi & Kataoka, 2008; O'Brien et al., 2001), the solar wind proton density (Balikhin et al., 2011; Borovsky & Denton, 2010; Lyatsky & Khazanov, 2008; Lyons et al., 2005), the auroral activity measured by the *AE* index (Hajra et al., 2015; Kim et al., 2015; Li et al., 2009; Meredith, 2002; Meredith, 2003), and the solar wind or magnetospheric ULF wave activity (Kim et al., 2006; Kozyreva et al., 2007; Potapov et al., 2014; Rostoker et al., 1998).

The physical processes that lead to the variations in relativistic electron fluxes in the outer radiation belt have been another important area of study. While the topic is still open, it is generally accepted that the main processes for relativistic electron losses are magnetopause shadowing (Turner et al., 2012), outward radial diffusion (Shprits et al., 2006), and pitch angle scattering to the atmosphere (Gao et al., 2015; Hyun et al., 2014; Thorne et al., 2013). For electron acceleration leading to an increase in relativistic electron fluxes, we point to wave-particle interactions (Bortnik & Thorne, 2007; Horne et al., 2007; Summers et al., 1998; Thorne, 2010) acting on a seed population and resonance with ULF wave activity (Mathie & Mann, 2000; Mann et al., 2013) as the main causes. Understanding the processes that lead to variability is a major goal of radiation

belt research. However, when it comes to applications, and in particular prediction, we need a better understanding of the external factors driving the relativistic electron fluxes, as it has become clear that elevated fluxes can damage satellites in geostationary orbit (Baker, 2000; Wrenn, 2009; Wrenn et al., 2002), disrupt communications, and pose a threat for space exploration. Therefore, having the ability to predict the outer belt variability accurately has important technical applications and several efforts have been conducted in this regard (Baker et al., 1990; Boynton et al., 2015; Li et al., 2001; McPherron et al., 2009; Reeves, 1998; Simms et al., 2014, 2016; Turner & Li, 2008).

Relativistic electron flux variations have been historically associated with geomagnetic storms (e.g., Gonzalez et al., 1994), with a common proposition that storms are accompanied by a drop in the electron flux during the storm main phase followed by a recovery or increase during the storm recovery phase (e.g., Reeves, 1998). Even though this association is relatively common, not all storms result in enhancements from prestorm levels. For example, Reeves et al. (2003) studied 276 storms and only 53% were associated with an enhancement event at geostationary orbit, while 19% were associated with a net flux loss and 28% showed no significant change. Similar results have been obtained in other studies (e.g., Moya et al., 2017; Turner et al., 2013; Zhao & Li, 2013), giving us confirmation that storms are not always associated with enhancement or depletion in relativistic electron fluxes.

To better understand the geomagnetic conditions needed for the fluxes of relativistic electrons to be enhanced or depleted, it is very important to study the problem from a non *Dst*-based point of view. By using *Dst* minima during storm to locate events, we restrict the studies to only a subset of all events and therefore limit our capacity to fully understand the enhancement and depletion phenomena and to develop fully functional predictive capabilities. For example, starting from enhancement events, Kim et al. (2015) showed that a geomagnetic storm, as defined by a drop in *Dst* index, is not necessary for a relativistic electron enhancement event to occur and that a persistent southward interplanetary magnetic field (IMF) or north-south IMF oscillations that can drive sufficiently large substorm activity as measured by *AE* index are key for enhancements occurrence (see also Hajra et al., 2015; Rodger et al., 2016, and references therein).

In this work, we study two types of events associated with flux variations: relativistic electron enhancement events and relativistic electron persistent depletion events that occurred during the years between 1996 and 2006. We examine various solar wind parameters that are associated with them to understand if there are critical parameters involved in the processes of enhancement or persistent depletion. Section 2 describes the event selection criteria and the data used for the study. Section 3 presents the results of a superposed epoch analysis of the events and cumulative distribution analysis for various solar wind parameters for both enhancement and persistent depletion events and the comparison between them. Section 4 discusses some ideas about the predictability of relativistic electron enhancement events and persistent depletion events based on our results.

2. Selection of Events and Data

We use >2 MeV electron flux data sampled at 5 min by the Energetic Particle Sensor (EPS) instrument on board the Geostationary Operational Environmental Satellite (Onsager et al., 1996) GOES 8 (1996–2003), and GOES 10 (2003–2006) satellites located at geostationary orbit to identify the events to study, and GOES 11 (2007–2010) to test the predictive power of the results. To avoid background contamination from energetic solar protons, we have used NOAA definition of solar proton events of >10 cm^{-2} sr^{-1} s^{-1} in the >10 MeV proton channel as a criterion for exclusion if they were measured during the first 2 days following the start of our events. Relativistic electron enhancement events (REE) are defined by an increase in the minimum daily flux from less than 10^2 cm^{-2} sr^{-1} s^{-1} to more than 2×10^3 cm^{-2} sr^{-1} s^{-1} in less than 48 h, followed by an average daily flux larger than 0.5×10^3 cm^{-2} sr^{-1} s^{-1} for at least 3 days and a relative increase of at least a factor of 4 for the flux daily average. Time $t = 0$ corresponds to the time when the increase in flux initiates. Relativistic electron persistent depletion events (REPDE) are defined as a drop to less than 10^1 cm^{-2} sr^{-1} s^{-1} in the maximum daily flux resulting in a decrease of a factor of 4 or more with respect to the predrop flux and with daily average flux remaining below 10^1 cm^{-2} sr^{-1} s^{-1} for at least 3 days. For REPDE, time $t = 0$ is determined by the time at which flux reaches its minimum value after the initial drop. Figure 1 shows a schematic of the electron flux evolution for REE and REPDE. During the period covered by this study, from 1996 to 2006, we identified 61 REE and 21 REPDE.

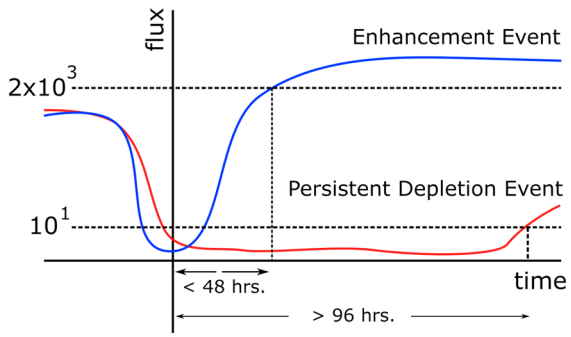

Figure 1. Scheme of the flux evolution for an idealized relativistic electron enhancement event (red) and a relativistic electron persistent depletion event (blue). The parameter $t = 0$ corresponds to the time when the enhancement can be first appreciated (REE) or when the depletion is complete (REPDE), vertical dashed lines represent the time in which threshold value should be reached for REE and the minimum duration allowed for persistent depletions.

To study solar wind parameters, we use the OMNI database that provides 1 min temporal resolution data obtained from ACE, Wind, and IMP-8 satellites processed to be shifted to the position of the Earth's bow shock nose and that can be obtained through CDAWeb (http://cdaweb.gsfc.nasa.gov). IMF ULF index corresponds to a 1 h average of the spectral power in the Pc5 range (1–8 mHz) calculated from Wind, ACE, and IMP-8 1 min resolution IMF data time shifted to the magnetopause nose using the method of Kozyreva et al. (2007), and the data can be obtained from the Augsburg website (http://space.augsburg.edu/MACCS/ULF_index). IMF ULF power is then calculated as 10^{index} with a 1 h resolution.

We have also cataloged the events by their associated solar driver, that is, interplanetary coronal mass ejection (CME) or corotating interaction region (CIR). The identification of the solar wind driver was based on the observation of solar wind speed changes (V_x and V_y), proton density changes, and IMF B_z response around the time of the events. For REE, 53 events are associated with a CIR and 8 with a CME, while for REPDE, 18 are associated with a CIR and 3 with a CME. The full list of events with their respective start times can be found in the supporting information.

3. Superposed Epoch Time Analysis

Figure 2 shows an example of a relativistic electron enhancement event that occurred on 29 June 2004 (left) and a relativistic electron persistent depletion event that occurred on 16 January 1998 (right). For both events, we also show the different parameters that are considered in this work; from top to bottom, solar wind speed V_x, solar wind proton density n_{sw}, solar wind dynamic pressure p_{dyn}, interplanetary magnetic field B_z, *AE* index, IMF ULF power, and solar wind reconnection electric field E_y component (Kan & Lee, 1979). Note that the *SYM-H* index has been deliberately excluded because we collected our events without considering *SYM-H* drops. To examine a possible *SYM-H* influence, Figure 3 shows the time difference between the *SYM-H* minimum value for each individual event and the time we have labeled as $t = 0$. Negative values indicate that *SYM-H* minimum occurred before time $t = 0$. We have indicated in red the events associated with a CME and in blue those associated with a CIR. While a spread in time is expected, it is interesting to note that relativistic enhancement event can start before *SYM-H* minimum when that minimum is modest, and there are several enhancement events for *SYM-H* minimum > -50 nT, which are not traditionally considered as geomagnetic storms. For persistent depletion events, we would expect the *SYM-H* minimum to occur at positive time (after flux minimum), if we assume depletions occur during the storm main phase. However, this is not true for all our events as can be seen in the figure. Figure 3 is consistent with results that magnetic storms are not directly related to relativistic electron enhancements at geostationary orbit, (Hajra et al., 2015; Kim et al., 2015), as events can happen at any time relative to, and for any value of, *SYM-H* minimum. While the occurrence of geomagnetic storm was not a criterion for event selection, we note that all REE are associated with some type of geomagnetic disturbance.

Figure 4 shows a superposed epoch time analysis of the solar wind and magnetospheric parameters displayed in Figure 2 to statistically identify common features that are associated with the relativistic electron enhancement events. Every individual event is shown in light grey to illustrate the spread of each parameter. The upper and lower quartile values are shown in blue and the median values in red. The top panel in Figure 4 shows the time evolution of the >2 MeV electron flux, and we can observe the statistical shape of an enhancement modulated by the magnetic local time dependence (diurnal variation) of the flux. For negative time, the flux oscillates in the range 10^0 to 10^2 cm^{-2} sr^{-1} s^{-1}. At time $t = 0$ the enhancement in flux starts, and in the first 12 h each quartile value rapidly increases by 2 orders of magnitude. Within 36 h after the enhancement initiation, the ratio of the flux levels to preflux values is larger than 3 orders of magnitude. Around this time, we consider the enhancement to have stopped, despite some minor growth in flux during the following days for some events. When analyzed separately, events associated with a different solar wind driver, CIR or CME disturbances, exhibit very similar behaviors, suggesting that the overall average enhancement characteristic does not depend on the type of driver (CME and CIR separated superposed epoch analysis are provided in the supporting information). The solar wind speed V_x component shows a continuous increase

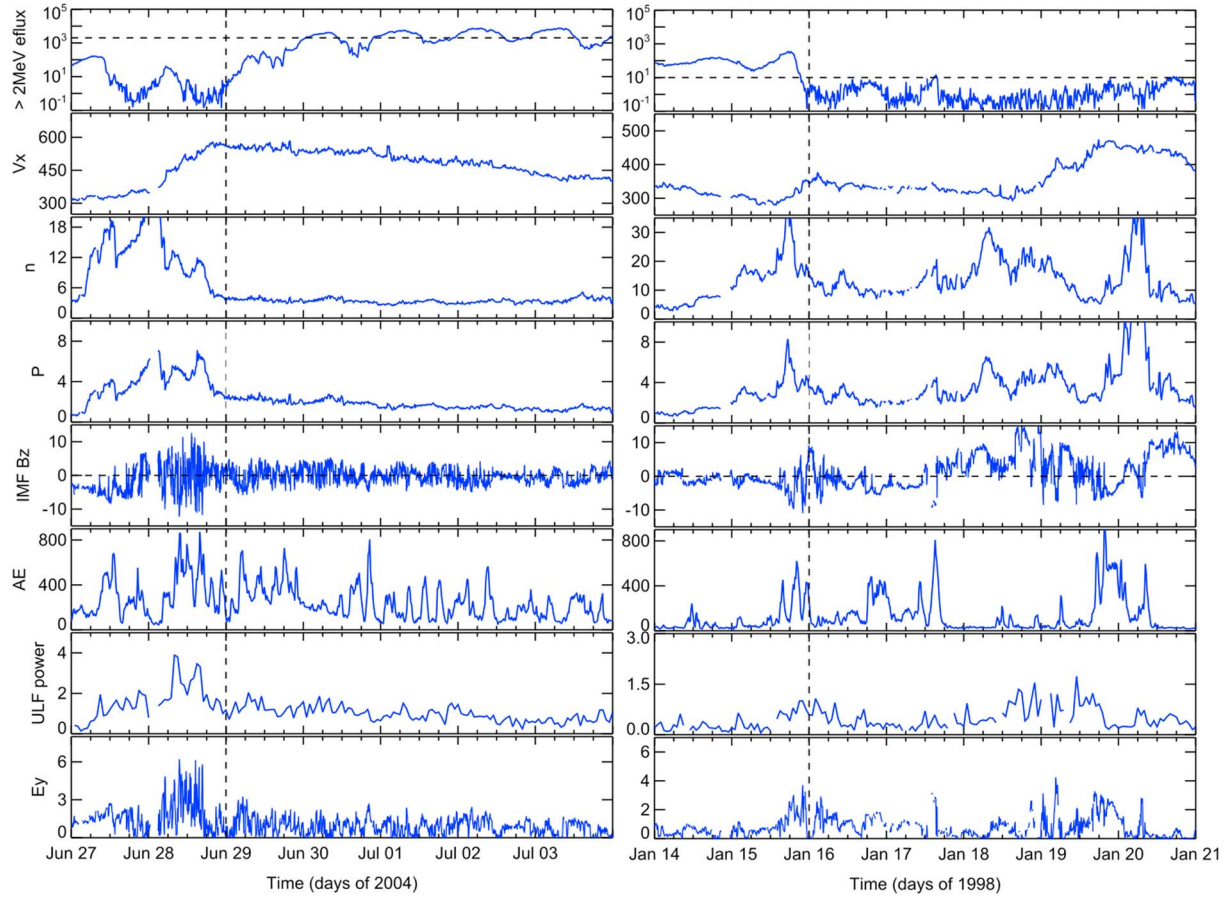

Figure 2. Example of a (left) relativistic electron enhancement event that occurred on 29 June 2004 and (right) persistent depletion event that occurred on 16 January 1998. From top to bottom, panels show >2 MeV electron flux (cm^{-2} sr^{-1} s^{-1}) from GOES, solar wind speed V_x (km/s), solar wind proton density n (cm^{-3}), solar wind dynamic pressure p_{dyn} (nPa), interplanetary magnetic field (IMF) B_z (nT), *AE* index (nT), solar wind ULF power (nT^2), and solar wind reconnection electric field E_y (mV/m). Vertical dashed line indicates the time $t = 0$ enhancement start or depletion of flux.

that reaches a maximum soon after the enhancement starts and then a plateau, with the speed not decreasing for most of the duration of events. The lower quartile has a speed >500 km/s for the whole duration of the enhancement events.

Solar wind proton density n_{sw} and solar wind dynamic pressure p_{dyn} both show a drop right before the enhancement starts. A further relevant feature is that for the duration of the enhancement period, both solar wind proton density and dynamic pressure values remain low and recover only when electron fluxes start to decrease. Interplanetary magnetic field B_z magnitude for preenhancement is larger than postenhancement and presents strong ULF oscillations due to the compression in the solar wind stream interface (as the majority of events are associated with CIRs). The oscillations and the magnitude of B_z are much weaker during the flux enhancement period. B_z median value is slightly southward directed with $0 > B_z > -1$ nT during that same period. For derived indices, *AE* index peaks around the time enhancements start at around 400 nT and remains elevated for most of the preenhancement and postenhancement time period. ULF power peaks around half a day before the enhancement starts and steadily decreases afterward. The peak ULF power median value is double the average (~0.79 nT^2) and median (~0.82 nT^2) ULF power that characterizes the 11 year period of this study, and the power decreases until it reaches average values a few days following the enhancement Finally, the reconnection electric field calculated from the definition given by Kan and Lee (1979) increases and peaks in a similar way to ULF power. Considering that reconnection electric field is an indicator of magnetospheric convection, it makes sense to expect an increase in electric field before the enhancement in flux begins (Hwang et al., 2007; Kissinger et al., 2014; Lyons et al., 2005, 2009; Meredith, 2002).

Figure 5 shows the relativistic electron persistent depletion events following the same format as Figure 4. Epoch $t = 0$ is the time where the flux has dropped to its minimum (or below instrument background).

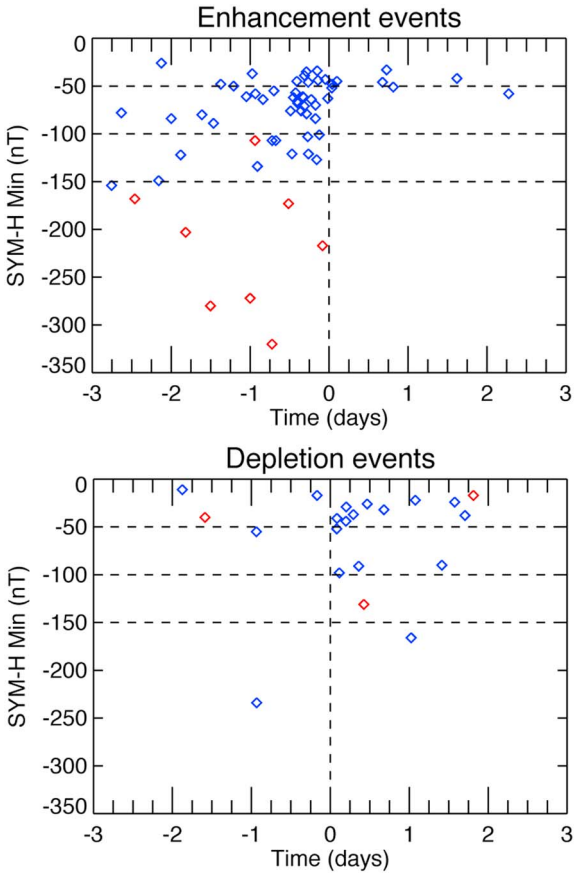

Figure 3. Minimum *SYM-H* value for (top) enhancement events and (bottom) dropouts and their time of occurrence with respect to start time $t = 0$. Red marks indicate CME events and blue marks indicate CIR events. Horizontal dashed lines indicate traditional definitions of weak (−50 nT), moderate (−100 nT), and strong (−150 nT) geomagnetic storms.

Maybe the most important feature in Figure 5 is that for almost 4 days no recovery exists, the shortest individual event lasting 3.7 days. Solar wind speed V_x has a median value $V_x < 400$ km/s and very few cases show speeds closer to $V_x \sim 450$ km/s. There are only three persistent depletion events associated with CME, and those have a higher speed $V_x \sim 500$ km/s (see supporting information for differentiated superposed epoch analysis), which suggest that for persistent depletion events, the solar wind speed might have a different impact depending on whether the event is associated with CME or CIR. Large peaks in solar wind proton density n_{sw} and solar wind dynamic pressure are observed around the time the drop in flux occurs, a result that agrees with a possible depletion through magnetopause shadowing (Hietala et al., 2014; Kim et al., 2010; Shprits et al., 2006; Turner et al., 2012). There is a drop in both dynamic pressure and proton density in the following days, but the values are still very large compared to those seen in enhancement events, suggesting that a low versus high value in dynamic pressure and/or proton density is important for the differentiation of the two types of events. IMF B_z median value is negative (southward directed) around the time flux drops and is followed by a northward B_z turning just after time $t = 0$. This northward oriented B_z median lasts for several days, and only around the fourth day after the persistent depletion event started does the median value return to a near zero value. If a jump in proton density and dynamic pressure might explain in part the initial drop, the combination of low solar wind speed and northward directed B_z might explain why the flux does not recover. *AE* index is significantly low except for a small increase around the time the drop occurs, providing another possible explanation for lack of electron flux recovery due to the lack of seed population injection to the radiation belts (e.g., Jaynes et al., 2015). IMF ULF power remains relatively near its average value (~0.79 nT^2), the main difference with respect to enhancement events being the lack of a pre-$t = 0$ increase. The reconnection electric field also is low during the time of the drop, having a small increase just at the drop time and then several days later.

To further characterize the relationship between the solar wind (together with magnetospheric parameters) and relativistic electron enhancement and persistent depletion events, in Figure 6 we have calculated cumulative distributions for the parameters presented in Figures 4 and 5. Figure 6 shows relativistic electron enhancement events (blue) and relativistic electron persistent depletion events (red) cumulative distribution of the average value for the day before the start time (dashed line) and for the day after the events started (solid line). (Figure 6a) shows solar wind speed, and we have drawn a dotted black line at $V_x = 520$ km/s that corresponds to the point of maximum separation between enhancement events and persistent depletion events. After time $t = 0$, 90% of events have a velocity above (enhancement) or below (persistent depletion) this chosen speed value. Both enhancement and persistent depletion events occur with an increase in solar wind speed, but the difference in values exceeding 100 km/s is a clear indication and further confirmation that a high solar wind speed characterizes all relativistic electron enhancement events and is likely necessary for relativistic electron enhancement events to occur. Solar wind proton density (Figure 6b) presents a clear decrease in value between the preenhancement and the postenhancement time for enhancement events but not for persistent depletion events. We have drawn a dashed line at $n_{sw} = 4$ cm^{-3} for solar wind proton density as that value separates more than 90% of the enhancement events between a pretime and posttime $t = 0$. In the case of the persistent depletion events, we notice that most events are associated with large solar wind proton density values. For solar wind dynamic pressure, shown in Figure 6c, we can also find a similar separation value for pretime and posttime $t = 0$ in relativistic electron enhancement events. Choosing $p_{dyn} = 3$ nPa separates around 80% of the enhancement events, indicating that a drop in p_{dyn} is a very common feature for REE. Looking at persistent depletion events, we notice that the cumulative distribution falls right in between the distributions for pretime and posttime $t = 0$ of relativistic electron enhancement events and presents

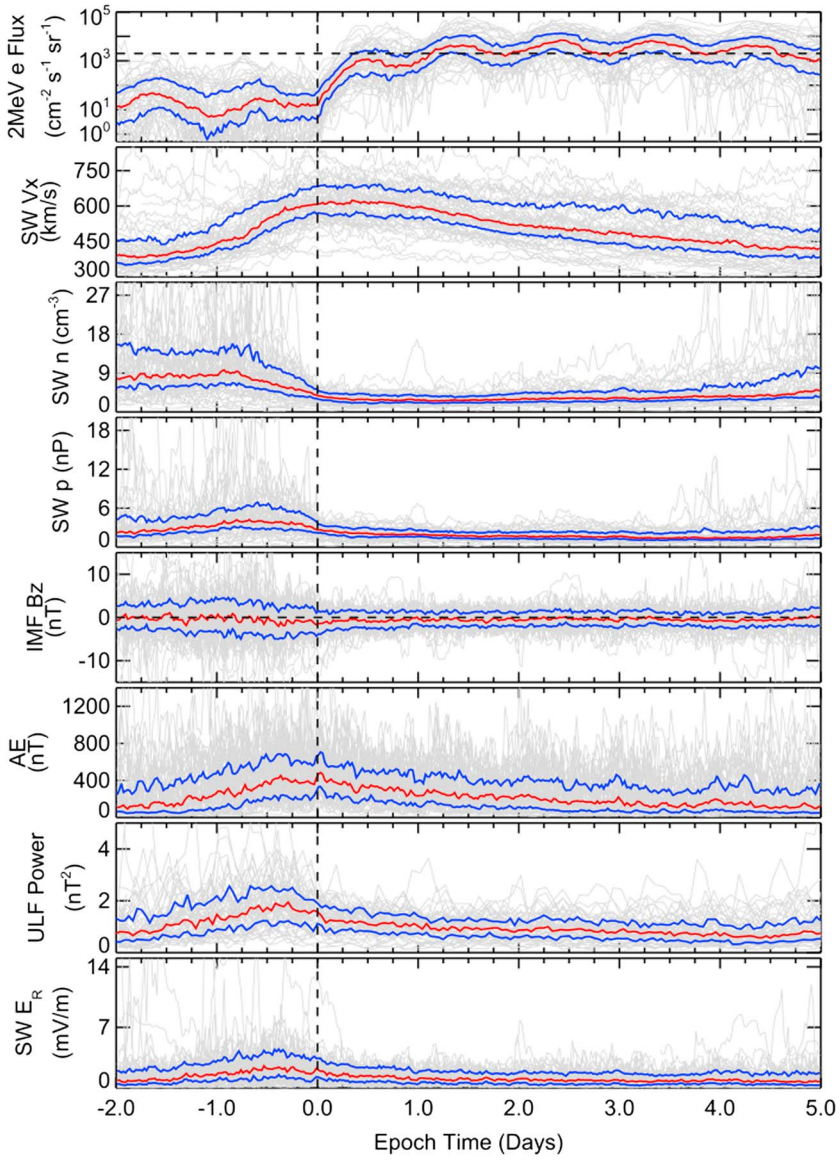

Figure 4. Epoch time superposition of 61 relativistic electron enhancement events. Median value of events is shown in red, and upper and lower quartile values are shown in blue. Light gray background corresponds to every single superposed event. From top to bottom, panels show >2 MeV electron flux from GOES, solar wind speed V_x, solar wind proton density, solar wind dynamic pressure, interplanetary magnetic field (IMF) B_z, *AE* index, IMF ULF power, and solar wind reconnection electric field.

little change. That the cutoff value is not as clear for solar wind dynamic pressure when compared with solar wind proton density suggests that solar wind proton density is a better parameter to characterize the events than solar wind dynamic pressure and possibly has better predictive potential. The *AE* index (Figure 6d) shows little variation around $t = 0$ for enhancement events, which in combination with Figure 4 indicates a very steady disturbance during preenhancement and postenhancement, with 90% of events having $AE > 250$ nT. High *AE* index has been proposed a necessary condition for REE to occur (Hajra et al., 2015; Jaynes et al., 2015; Kim et al., 2015), as it reflects energy transfer from the solar wind to the magnetosphere and can be associated with injection of seed populations to geostationary orbit. Similarly, persistent depletion events also show very little variation around $t = 0$, but around 80% of these events have $AE < 250$ nT.

To characterize IMF B_z, we have estimated the percent of the time IMF B_z is pointing southward in GSM coordinates and the hourly average value of the southward component. Figure 6e shows the percent of time that IMF B_z is pointing southward and the black dashed line is set at 50%, This roughly separates 80% of the

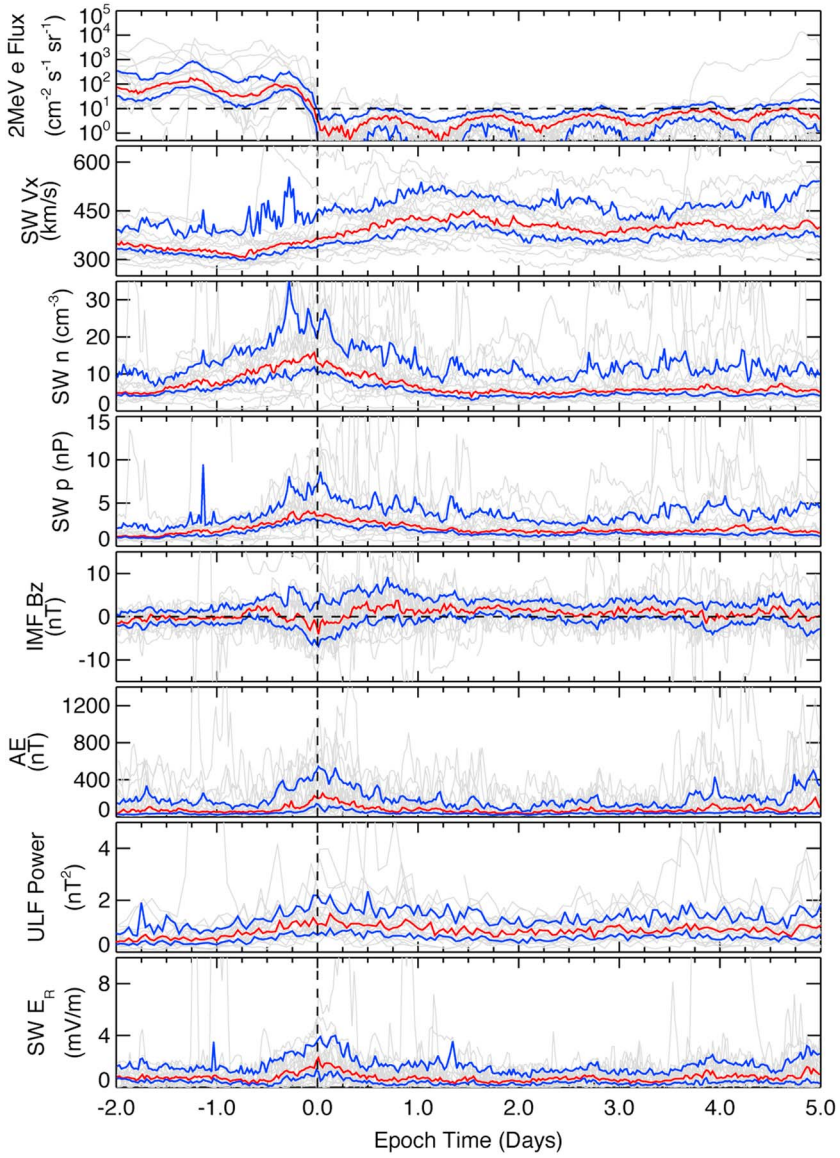

Figure 5. Epoch time superposition of 21 relativistic electron depletion events. Median value of events is shown in red, and upper and lower quartile values are drawn in blue. Light gray background corresponds to every single superposed event. From top to bottom, panels show >2 MeV electron flux from GOES, solar wind speed V_x, solar wind proton density, solar wind dynamic pressure, interplanetary magnetic field (IMF) B_z, *AE* index, IMF ULF power, and solar wind reconnection electric field.

enhancement events (more than 50% of the time pointing southward) and persistent depletion events (less than 50% of the time pointing southward) for both pre- and post-$t = 0$. This indicates the dominance of a southward oriented B_z during enhancement events. To determine the characteristic values associated with the predominantly southward IMF, the absolute value of the hourly averaged southward directed Bz is shown in Figure 6f. A dashed line has been selected at $B_z = 2$ nT. Around 80% of the events are below that number after the enhancement starts. In this case, the most intense southward IMF occurs before the enhancement time $t = 0$ and it seems to decrease afterward. The postenhancement southward IMF B_z values are similar to the persistent depletion southward IMF B_z values. Both Figures 6e and 6f suggest that continuous occurrence of south oriented IMF B_z, which is not necessarily large in value, is important in driving strong electron enhancement. Figure 6g shows the reconnection electric field and the cumulative plot is very similar to IMF B_z, that is, for REE it decreases after $t = 0$ and reaches levels similar to those seen in persistent depletion events. ULF power also shows a decrease indicating that the fluctuations in the IMF are less intense during the

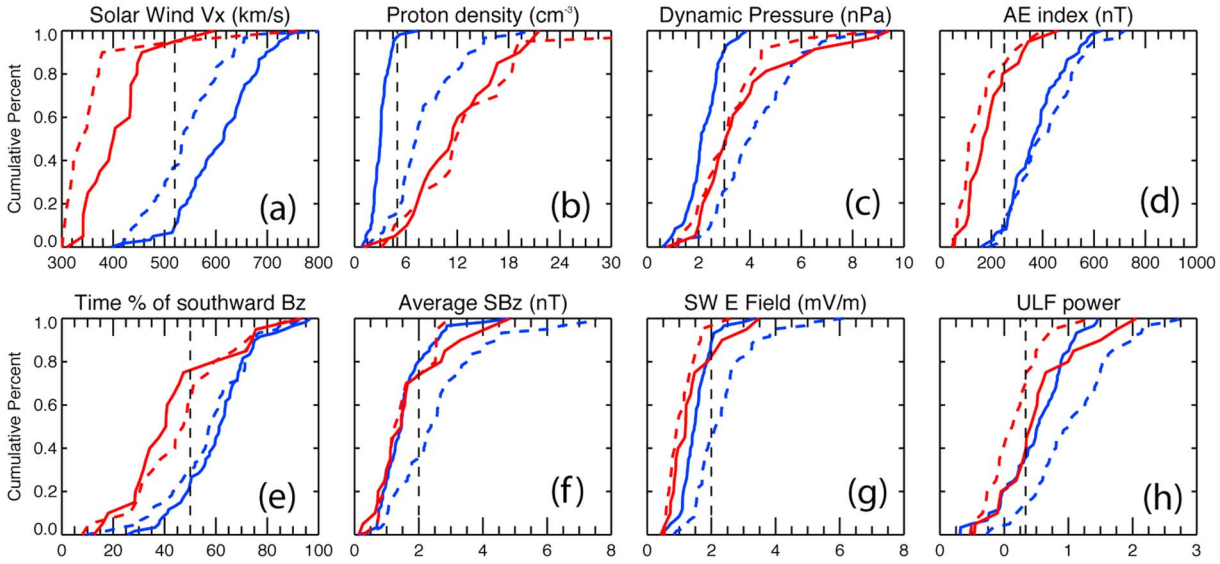

Figure 6. Cumulative distribution functions associated with REEs (blue) and persistent depletion events (red). Dashed lines correspond to the average of the 24 h period before the beginning of the event at $t = 0$, and solid lines correspond to the average of the 24 h period after $t = 0$. The eight different panels correspond to (a) solar wind speed V_x, (b) solar wind proton density, (c) solar wind dynamic pressure, (d) *AE* index (e) time percent of southward directed IMF B_z, (f) average southward IMF B_z, (g) solar wind reconnection electric field, and (h) IMF ULF power.

period that follows the start of the enhancement. The bottom panels in Figure 6 seem to indicate that IMF B_z magnitude and oscillations may be important in the process that leads to enhancement but of no significant importance in the process that leads to the persistent depletion.

4. Summary and Discussion

We have epoch analyzed a set of relativistic electron enhancement and persistent depletion events that occurred between the years 1996 and 2006, identified using >2 MeV electron flux observations at geostationary orbit from GOES 8 and GOES 10 spacecraft. Our results are consistent with previous results (e.g., Paulikas & Blake 1979; Reeves et al., 2011) in that a large average solar wind speed ($V_x > 500$ km/s) is characteristic of enhancement events. We have also found that persistent depletion events are characterized by lower solar wind speeds ($V_x < 450$ km/s) that are still associated with some type of geomagnetic disturbance (CIR or CME). When comparing REE to REPDE, we find that a threshold velocity separates relativistic electron events from persistent depletion event. Our current estimated threshold value is $V_x = 520$ km/s for which more than 90% of events are situated above (enhancement) or below (persistent depletion). A similar result is obtained for solar wind proton density, where we identify a separation value between relativistic enhancement events and persistent depletion events. A low solar wind proton density seems to be needed for the enhancements to occur (no enhancement event occurs for $n_{sw} > 4$ cm^{-3}), A value of $n_{sw} = 4$ cm^{-3} around $t = 0$ is sufficient to differentiate an enhancement event from a persistent depletion event in most cases. Our results do not suggest that a low solar wind proton density is a sufficient condition to ensure that an enhancement event will occur but strongly suggest that it is a necessary condition for one to occur. Solar wind dynamic pressure closely follows the proton density. We can also find a pressure value to characterize relativistic electron enhancement occurrence, that value being $p_{dyn} = 3$ nPa. However, solar wind dynamic pressure is also tied to solar wind speed, so a low solar wind speed can also result in a low solar wind dynamic pressure, which is not favorable for REE occurrence, and therefore low p_{dyn} is not as reliable a predictor of relativistic electron enhancement events as solar wind proton density. IMF B_z is predominantly southward oriented for enhancement events and northward oriented for persistent depletion events. The strength of the magnetic field varies considerably from enhancement to persistent depletion events before time $t = 0$ but is similar after $t = 0$, therefore making a large southward oriented IMF B_z average a good indicator of a possible relativistic electron enhancement event. Reconnection electric field and *AE* values increase as the IMF B_z becomes more southward oriented, and peak around or right before $t = 0$. Increase in IMF fluctuations as shown in the ULF power index are characteristic of the period of preenhancement and remain above their average value during the period of flux enhancement.

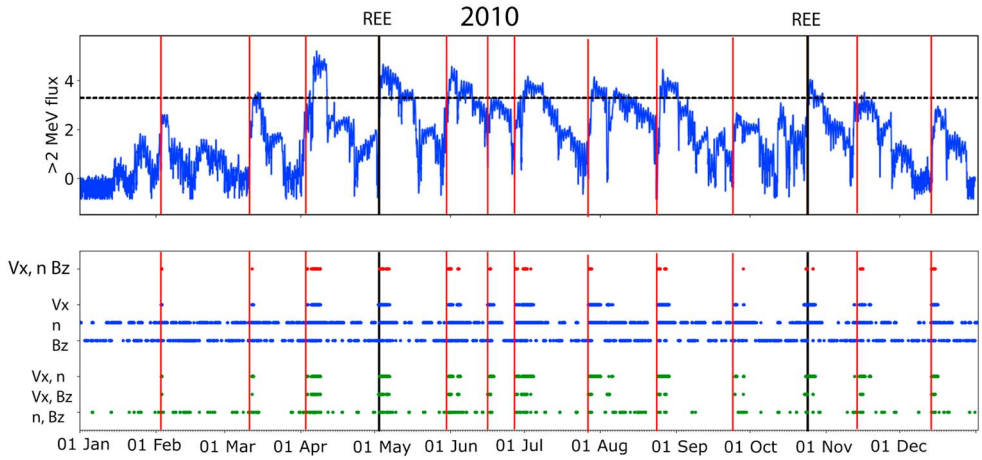

Figure 7. Yearly >2 MeV flux from GOES (top) for year 2010 and different thresholds: solar wind speed $V_x > 520$ km/s, solar wind proton density $n_{sw} < 4$ cm^{-3}, and IMF B_z southward component average $\langle B_z \rangle < -2$ nT. Colors indicate when three thresholds are met (red), two different thresholds are met in different combinations (green), or one is met (blue). Black vertical lines correspond to REE and red vertical lines correspond to a period in which the three thresholds are met and an enhancement (not considered REE) occurs.

In general, our results agree really well with the results of previous works that have focused only on events associated with storms and with those that study long-term variations of the electrons at geostationary orbit. We have gone one step further and established a set of thresholds for some solar wind parameters that we expect will be of use to predict relativistic electron enhancement events. We note that these parameters are not the only possible predictors. *AE* index and reconnection electric fields could be used, but these relate strongly to IMF B_z and solar wind speed and thus would not add new information. *SYM-H* is not a reliable predictor as a decrease in *SYM-H* is not needed for a relativistic electron event to occur. Instead, a disturbance associated with a corotating interaction region might result in an enhancement just as during a storm recovery phase independent of whether the event led to a significant *SYM-H* drop (see also Miyoshi & Kataoka, 2008).

For a simple test of predictive power of our results we have set up a simple set of conditions using a threshold mechanism. According to our results, we expect an enhancement event to occur when $V_x > 520$ km/s, $n_{sw} < 4$ cm^{-3}, and southward average $B_z < -2$ nT. Going through the period of our study, 1 January 1996 to 31 December 2006, we find that 90% (55 of 61 events) fulfill the three conditions, while in the other six at least two are met. We have extended this testing to the out-of-study period from 1 January 2007 to 31 December 2010 during which our identification criterion gives 18 relativistic electron enhancement events. The set of threshold conditions is able to predict 16 of those 18 events, while the two missing still fulfill at least two of the three conditions. Figure 7 show the predictability during the year 2010 using different combinations of thresholds as identified in the lower panel. Interestingly, in 2010 we have only two relativistic electron enhancement events based on the criteria we used to select them, yet there are plenty of increases in flux that we have not cataloged as events but the threshold criteria account for all of them. We are showing 2010 as it is a particularly inactive year, together with 2009, as they are close to solar minimum. This may present some extra challenges when it comes to prediction (Rodger et al., 2016); however, visualization is easier. The identification of relativistic electron enhancement events and increases in flux not labeled as "events" still works for the years not shown on the plot. Therefore, although this is a rather simple attempt, it strongly indicates that a combination of the high solar wind speed, low solar wind proton density, and southward IMF is important in the electron acceleration process regardless of the detailed physical mechanisms for acceleration.

We have also studied IMF ULF as a possible contributor to relativistic electron enhancement events, specifically when IMF B_z is not strong enough to result in enhancement as was proposed by Kim et al. (2006). While the cumulative distribution analysis did not show clear statistically relevant signature in IMF ULF power other than an increase just before $t = 0$, we think that in a case by case study, IMF ULF power can provide some extra information to improve predictive capabilities. Figure 8 compares a relativistic electron enhancement event with steady, relatively large southward IMF B_z (left) and an event with north-south fluctuating IMF with average B_z close to 0 (right). Despite the large difference in average southward B_z, the electron intensities reach comparable peaks. This observation suggests that north-south ULF fluctuations might be as effective

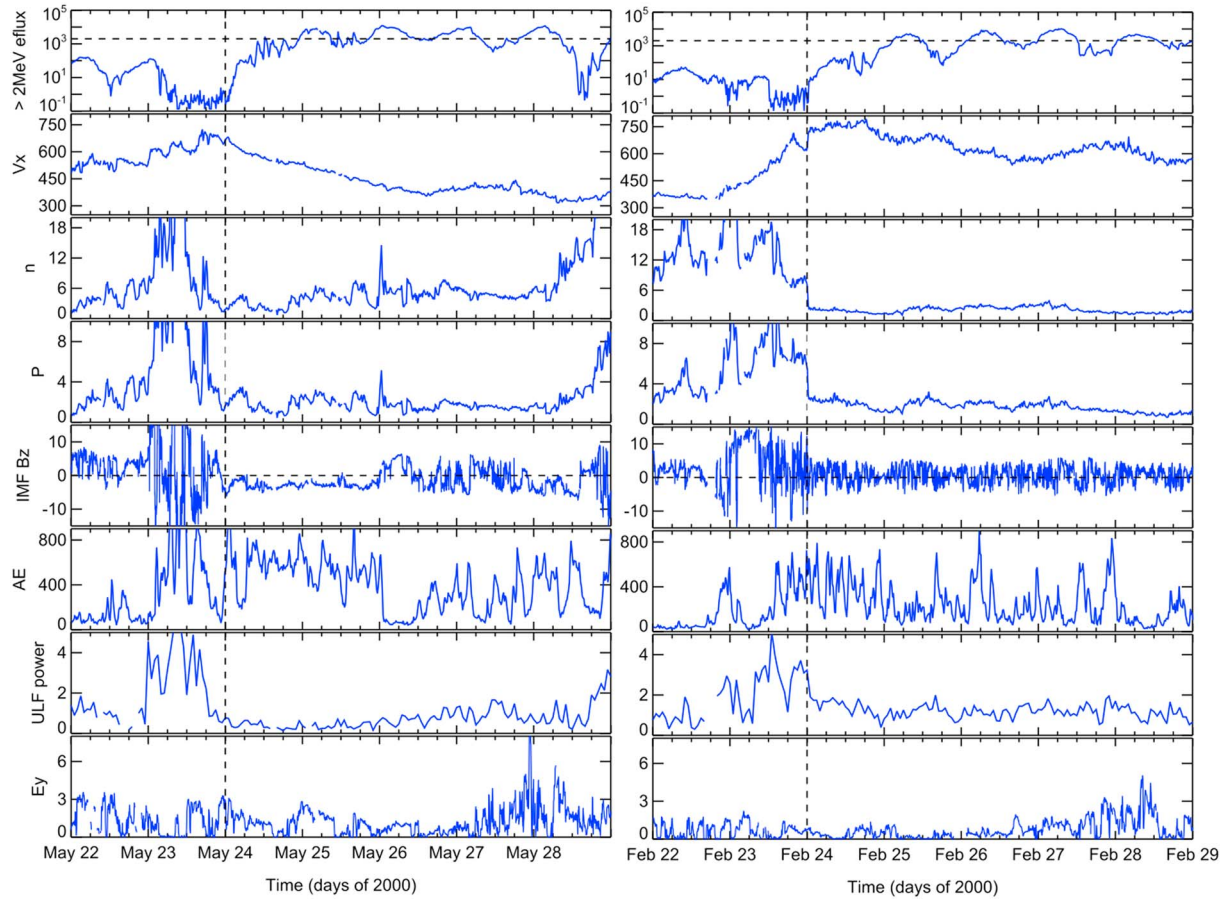

Figure 8. Example of a relativistic electron enhancement event that occurred on (left) 24 May 2000 with a very steady IMF B_z component during the enhancement period and (right) 24 February 2000 that presents a minor IMF B_z component but intensely fluctuating, as captured by ULF index. From top to bottom, panels show >2 MeV electron flux from GOES, solar wind speed V_x, solar wind proton density, solar wind dynamic pressure, interplanetary magnetic field (IMF) B_z, *AE* index, solar wind ULF power, and solar wind reconnection electric field. Vertical dashed line indicates the time $t = 0$ enhancement start or depletion of flux.

as steady, relatively large southward IMF in transferring solar wind energy that can drive continuous *AE* activity which in turn drive electron enhancement at GEO by supplying seed electrons and contributing to the growth of waves that can accelerate the seed electrons via wave-particle interactions. This is a topic that we believe warrants further elaborated study. Statistical verification of an IMF ULF power effect requires separation of its effect from the effects of other solar wind parameters, especially solar wind speed, because large IMF fluctuations usually prevail in high-speed streams and IMF ULF power effect can only be secondary to the dominant solar wind speed effect.

Acknowledgments
Victor Pinto would like to thank the support from Becas Chile fellowship program. H.J. Kim is thankful for support from NASA grant NNX14AD18G. Jacob Bortnik would like to acknowledge support from NASA grant NNX14AN85G and AFOSRFA9550-15-1-015. GOES data and OMNI data are available at the Coordinated Data Analysis Web (CDAWeb) (http://cdaweb.gsfc.nasa.gov/). ULF data is available at the Augsburg website (http://space.augsburg.edu/MACCS/ULF_index).

References

Baker, D., Li, X., Blake, J., & Kanekal, S. (1998). Strong electron acceleration in the Earth's magnetosphere. *Advances in Space Research*, *21*(4), 609–613. https://doi.org/10.1016/S0273-1177(97)00970-8

Baker, D. N. (2000). The occurrence of operational anomalies in spacecraft and their relationship to space weather. *IEEE Transactions on Plasma Science*, *28*(6), 2007–2016.

Baker, D. N., Blake, J. B., Klebesadel, R. W., & Higbie, P. R. (1986). Highly relativistic electrons in the Earth's outer magnetosphere: 1. Lifetimes and temporal history 1979–1984. *Journal of Geophysical Research*, *91*(A4), 4265. https://doi.org/10.1029/JA091iA04p04265

Baker, D. N., McPherron, R. L., Cayton, T. E., & Klebesadel, R. W. (1990). Linear prediction filter analysis of relativistic electron properties at 6.6 R_E. *Journal of Geophysical Research*, *95*(A9), 15,133–15,140. https://doi.org/10.1029/JA095iA09p15133

Balikhin, M. A., Boynton, R. J., Walker, S. N., Borovsky, J. E., Billings, S. A., & Wei, H. L. (2011). Using the NARMAX approach to model the evolution of energetic electrons fluxes at geostationary orbit. *Geophysical Research Letters*, *38*, L18105. https://doi.org/10.1029/2011GL048980

Blake, J. B., Baker, D. N., Turner, N., Ogilvie, K. W., & Lepping, R. P. (1997). Correlation of changes in the outer-zone relativistic-electron population with upstream solar wind and magnetic field measurements. *Geophysical Research Letters*, *24*(8), 927–929. https://doi.org/10.1029/97GL00859

Borovsky, J. E., & Denton, M. H. (2010). Magnetic field at geosynchronous orbit during high-speed stream-driven storms: Connections to the solar wind, the plasma sheet, and the outer electron radiation belt. *Journal of Geophysical Research*, *115*, A08217. https://doi.org/10.1029/2009JA015116

Bortnik, J., & Thorne, R. (2007). The dual role of ELF/VLF chorus waves in the acceleration and precipitation of radiation belt electrons. *Journal of Atmospheric and Solar-Terrestrial Physics*, *69*(3), 378–386. https://doi.org/10.1016/j.jastp.2006.05.030

Boynton, R. J., Balikhin, M. A., & Billings, S. A. (2015). Online NARMAX model for electron fluxes at GEO. *Annales Geophysicae*, *33*(3), 405–411. https://doi.org/10.5194/angeo-33-405-2015

Boynton, R. J., Mourenas, D., & Balikhin, M. A. (2016). Electron flux dropouts at Geostationary Earth Orbit: Occurrences, magnitudes, and main driving factors. *Journal of Geophysical Research: Space Physics*, *121*, 8448–8461. https://doi.org/10.1002/2016JA022916

Gao, X., Li, W., Bortnik, J., Thorne, R. M., Lu, Q., Ma, Q., … Wang, S. (2015). The effect of different solar wind parameters upon significant relativistic electron flux dropouts in the magnetosphere. *Journal of Geophysical Research: Space Physics*, *120*, 4324–4337. https://doi.org/10.1002/2015JA021182

Gonzalez, W. D., Joselyn, J. A., Kamide, Y., Kroehl, H. W., Rostoker, G., Tsurutani, B. T., & Vasyliunas, V. M. (1994). What is a geomagnetic storm? *Journal of Geophysical Research*, *99*(A4), 5771–5792. https://doi.org/10.1029/93JA02867

Hajra, R., Tsurutani, B. T., Echer, E., Gonzalez, W. D., & Santolik, O. (2015). Relativistic (E > 0.6, > 2.0, and > 4.0 MeV) Electron acceleration at geosynchronous orbit during high-intensity, long-duration, continuous *AE* activity (Hildcaa) events. *The Astrophysical Journal*, *799*(1), 39. https://doi.org/10.1088/0004-637X/799/1/39

Hietala, H., Kilpua, E. K. J., Turner, D. L., & Angelopoulos, V. (2014). Depleting effects of ICME-driven sheath regions on the outer electron radiation belt. *Geophysical Research Letters*, *41*, 2258–2265. https://doi.org/10.1002/2014GL059551

Horne, R. B., Thorne, R. M., Glauert, S. A., Meredith, N. P., Pokhotelov, D., & Santolík, O. (2007). Electron acceleration in the Van Allen radiation belts by fast magnetosonic waves. *Geophysical Research Letters*, *34*, L17107. https://doi.org/10.1029/2007GL030267

Hwang, J. A., Lee, D.-Y., Lyons, L. R., Smith, A. J., Zou, S., Min, K. W., … Park, Y. D. (2007). Statistical significance of association between whistler-mode chorus enhancements and enhanced convection periods during high-speed streams. *Journal of Geophysical Research*, *112*, A09213. https://doi.org/10.1029/2007JA012388

Hyun, K., Kim, K.-H., Lee, E., Kwon, H.-J., Lee, D.-H., & Jin, H. (2014). Loss of geosynchronous relativistic electrons by EMIC wave scattering under quiet geomagnetic conditions. *Journal of Geophysical Research: Space Physics*, *119*, 8357–8371. https://doi.org/10.1002/2014JA020234

Iles, R. H. A., Fazakerley, A. N., Johnstone, A. D., Meredith, N. P., & Bühler, P. (2002). The relativistic electron response in the outer radiation belt during magnetic storms. *Annales Geophysicae*, *20*, 957–965.

Jaynes, A. N., Baker, D. N., Singer, H. J., Rodriguez, J. V., Loto'aniu, T. M., Ali, A. F., … Reeves, G. D. (2015). Source and seed populations for relativistic electrons: Their roles in radiation belt changes. *Journal of Geophysical Research: Space Physics*, *120*, 7240–7254. https://doi.org/10.1002/2015JA021234

Kan, J. R., & Lee, L. C. (1979). Energy coupling function and solar wind-magnetosphere dynamo. *Geophysical Research Letters*, *6*(7), 577–580.

Kim, H.-J., Kim, K. C., Lee, D.-Y., & Rostoker, G. (2006). Origin of geosynchronous relativistic electron events. *Journal of Geophysical Research*, *111*, A03208. https://doi.org/10.1029/2005JA011469

Kim, H.-J., Lyons, L., Pinto, V., Wang, C.-P., & Kim, K.-C. (2015). Revisit of relationship between geosynchronous relativistic electron enhancements and magnetic storms. *Geophysical Research Letters*, *42*, 6155–6161. https://doi.org/10.1002/2015GL065192

Kim, K. C., Lee, D.-Y., Kim, H.-J., Lee, E. S., & Choi, C. R. (2010). Numerical estimates of drift loss and *Dst* effect for outer radiation belt relativistic electrons with arbitrary pitch angle. *Journal of Geophysical Research*, *115*, A03208. https://doi.org/10.1029/2009JA014523

Kissinger, J., Kepko, L., Baker, D. N., Kanekal, S., Li, W., McPherron, R. L., & Angelopoulos, V. (2014). The importance of storm time steady magnetospheric convection in determining the final relativistic electron flux level. *Journal of Geophysical Research: Space Physics*, *119*, 7433–7443. https://doi.org/10.1002/2014JA019948

Kozyreva, O., Pilipenko, V., Engebretson, M., Yumoto, K., Watermann, J., & Romanova, N. (2007). In search of a new ULF wave index: Comparison of Pc5 power with dynamics of geostationary relativistic electrons. *Planetary and Space Science*, *55*(6), 755–769. https://doi.org/10.1016/j.pss.2006.03.013

Li, L. Y., Cao, J. B., Zhou, G. C., & Li, X. (2009). Statistical roles of storms and substorms in changing the entire outer zone relativistic electron population. *Journal of Geophysical Research*, *114*, A12214. https://doi.org/10.1029/2009JA014333

Li, X., Baker, D. N., Temerin, M., Reeves, G., Friedel, R., & Shen, C. (2005). Energetic electrons, 50 keV to 6 MeV, at geosynchronous orbit: Their responses to solar wind variations. *Space Weather*, *3*, S04001. https://doi.org/10.1029/2004SW000105

Li, X., Temerin, M., Baker, D. N., Reeves, G. D., & Larson, D. (2001). Quantitative prediction of radiation belt electrons at geostationary orbit based on solar wind measurements. *Geophysical Research Letters*, *28*(9), 1887–1890. https://doi.org/10.1029/2000GL012681

Lyatsky, W., & Khazanov, G. V. (2008). Effect of solar wind density on relativistic electrons at geosynchronous orbit. *Geophysical Research Letters*, *35*, L03109. https://doi.org/10.1029/2007GL032524

Lyons, L., Lee, D.-Y., Kim, H.-J., Hwang, J., Thorne, R., Horne, R., & Smith, A. (2009). Solar wind-magnetosphere coupling, including relativistic electron energization, during high-speed streams. *Journal of Atmospheric and Solar-Terrestrial Physics*, *71*(10-11), 1059–1072. https://doi.org/10.1016/j.jastp.2008.04.016

Lyons, L. R., Lee, D.-Y., Thorne, R. M., Horne, R. B., & Smith, A. J. (2005). Solar wind-magnetosphere coupling leading to relativistic electron energization during high-speed streams. *Journal of Geophysical Research*, *110*, A11202. https://doi.org/10.1029/2005JA011254

Mann, I. R., Lee, E. A., Claudepierre, S. G., Fennell, J. F., Degeling, A., Rae, I. J., … Honary, F. (2013). Discovery of the action of a geophysical synchrotron in the Earth's Van Allen radiation belts. *Nature Communications*, *4*, 2795. https://doi.org/10.1038/ncomms3795

Mathie, R. A., & Mann, I. R. (2000). A correlation between extended intervals of ULF wave power and storm-time geosynchronous relativistic electron flux enhancements. *Geophysical Research Letters*, *27*(20), 3261–3264. https://doi.org/10.1029/2000GL003822

McPherron, R., Baker, D., & Crooker, N. (2009). Role of the Russell–McPherron effect in the acceleration of relativistic electrons. *Journal of Atmospheric and Solar-Terrestrial Physics*, *71*(10-11), 1032–1044. https://doi.org/10.1016/j.jastp.2008.11.002

Meredith, N. P. (2002). Outer zone relativistic electron acceleration associated with substorm-enhanced whistler mode chorus. *Journal of Geophysical Research*, *107*(A7), 1144. https://doi.org/10.1029/2001JA900146

Meredith, N. P. (2003). Evidence for chorus-driven electron acceleration to relativistic energies from a survey of geomagnetically disturbed periods. *Journal of Geophysical Research*, *108*(A6), 1248. https://doi.org/10.1029/2002JA009764

Miyoshi, Y., & Kataoka, R. (2008). Flux enhancement of the outer radiation belt electrons after the arrival of stream interaction regions. *Journal of Geophysical Research*, *113*, A03S09. https://doi.org/10.1029/2007JA012506

Moya, P. S., Pinto, V. A., Sibeck, D. G., Kanekal, S. G., & Baker, D. N. (2017). On the effect of geomagnetic storms on relativistic electrons in the outer radiation belt: Van Allen Probes observations. *Journal of Geophysical Research: Space Physics*, *122*, 11,100–11,108. https://doi.org/10.1002/2017JA024735

O'Brien, T. P., McPherron, R. L., Sornette, D., Reeves, G. D., Friedel, R., & Singer, H. J. (2001). Which magnetic storms produce relativistic electrons at geosynchronous orbit? *Journal of Geophysical Research*, *106*(A8), 15,533–15,544. https://doi.org/10.1029/2001JA000052

Onsager, T., Grubb, R., Kunches, J., Matheson, L., Speich, D., Zwickl, R. W., & Sauer, H. (1996). Operational uses of the GOES energetic particle detectors. *Proceedings of the SPIE*, *2812*, 281–290. https://doi.org/10.1117/12.254075

Paulikas, G., & Blake, J. (1979). Effects of the solar wind on magnetospheric dynamics: Energetic electrons at the synchronous orbit. In W. P. Olson (Ed.), *Geophysical Monograph Series* (pp. 180–202). Washington, DC: American Geophysical Union. https://doi.org/10.1029/GM021p0180

Potapov, A., Tsegmed, B., & Ryzhakova, L. (2014). Solar cycle variation of killer electrons at geosynchronous orbit and electron flux correlation with the solar wind parameters and ULF waves intensity. *Acta Astronautica*, *93*, 55–63. https://doi.org/10.1016/j.actaastro.2013.07.004

Reeves, G. D. (1998). Relativistic electrons and magnetic storms: 1992–1995. *Geophysical Research Letters*, *25*(11), 1817–1820. https://doi.org/10.1029/98GL01398

Reeves, G. D., McAdams, K. L., Friedel, R. H. W., & O'Brien, T. P. (2003). Acceleration and loss of relativistic electrons during geomagnetic storms. *Geophysical Research Letters*, *30*(10), 1529. https://doi.org/10.1029/2002GL016513

Reeves, G. D., Morley, S. K., Friedel, R. H. W., Henderson, M. G., Cayton, T. E., Cunningham, G., … Thomsen, D. (2011). On the relationship between relativistic electron flux and solar wind velocity: Paulikas and Blake revisited. *Journal of Geophysical Research*, *116*, A02213. https://doi.org/10.1029/2010JA015735

Rodger, C. J., Cresswell-Moorcock, K., & Clilverd, M. A. (2016). Nature's Grand Experiment: Linkage between magnetospheric convection and the radiation belts. *Journal of Geophysical Research: Space Physics*, *121*, 171–189. https://doi.org/10.1002/2015JA021537

Rostoker, G., Skone, S., & Baker, D. N. (1998). On the origin of relativistic electrons in the magnetosphere associated with some geomagnetic storms. *Geophysical Research Letters*, *25*(19), 3701–3704. https://doi.org/10.1029/98GL02801

Shprits, Y. Y., Thorne, R. M., Friedel, R., Reeves, G. D., Fennell, J., Baker, D. N., & Kanekal, S. G. (2006). Outward radial diffusion driven by losses at magnetopause. *Journal of Geophysical Research*, *111*, A11214. https://doi.org/10.1029/2006JA011657

Simms, L. E., Engebretson, M. J., Pilipenko, V., Reeves, G. D., & Clilverd, M. (2016). Empirical predictive models of daily relativistic electron flux at geostationary orbit: Multiple regression analysis. *Journal of Geophysical Research: Space Physics*, *121*, 3181–3197. https://doi.org/10.1002/2016JA022414

Simms, L. E., Pilipenko, V., Engebretson, M. J., Reeves, G. D., Smith, A. J., & Clilverd, M. (2014). Prediction of relativistic electron flux at geostationary orbit following storms: Multiple regression analysis. *Journal of Geophysical Research: Space Physics*, *119*, 7297–7318. https://doi.org/10.1002/2014JA019955

Summers, D., Thorne, R. M., & Xiao, F. (1998). Relativistic theory of wave-particle resonant diffusion with application to electron acceleration in the magnetosphere. *Journal of Geophysical Research: Space Physics*, *103*(A9), 20,487–20,500. https://doi.org/10.1029/98JA01740

Thorne, R. M. (2010). Radiation belt dynamics: The importance of wave-particle interactions: FRONTIER. *Geophysical Research Letters*, *37*, L22107. https://doi.org/10.1029/2010GL044990

Thorne, R. M., Li, W., Ni, B., Ma, Q., Bortnik, J., Baker, D. N., … Angelopoulos, V. (2013). Evolution and slow decay of an unusual narrow ring of relativistic electrons near L ˜ 3.2 following the September 2012 magnetic storm. *Geophysical Research Letters*, *40*, 3507–3511. https://doi.org/10.1002/grl.50627

Turner, D. L., & Li, X. (2008). Quantitative forecast of relativistic electron flux at geosynchronous orbit based on low-energy electron flux. *Space Weather*, *6*, S05005. https://doi.org/10.1029/2007SW000354

Turner, D. L., Angelopoulos, V., Li, W., Hartinger, M. D., Usanova, M., Mann, I. R., … Shprits, Y. (2013). On the storm-time evolution of relativistic electron phase space density in Earth's outer radiation belt. *Journal of Geophysical Research: Space Physics*, *118*, 2196–2212. https://doi.org/10.1002/jgra.50151

Turner, D. L., Shprits, Y., Hartinger, M., & Angelopoulos, V. (2012). Explaining sudden losses of outer radiation belt electrons during geomagnetic storms. *Nature Physics*, *8*(3), 208–212. https://doi.org/10.1038/nphys2185

Wing, S., Johnson, J. R., Camporeale, E., & Reeves, G. D. (2016). Information theoretical approach to discovering solar wind drivers of the outer radiation belt. *Journal of Geophysical Research: Space Physics*, *121*, 9378–9399. https://doi.org/10.1002/2016JA022711

Wrenn, G. (2009). Chronology of 'killer' electrons: Solar cycles 22 and 23. *Journal of Atmospheric and Solar-Terrestrial Physics*, *71*(10–11), 1210–1218. https://doi.org/10.1016/j.jastp.2008.08.002

Wrenn, G. L., Rodgers, D. J., & Ryden, K. A. (2002). A solar cycle of spacecraft anomalies due to internal charging. *Annales Geophysicae*, *20*, 953–956.

Zhao, H., & Li, X. (2013). Inward shift of outer radiation belt electrons as a function of *Dst* index and the influence of the solar wind on electron injections into the slot region. *Journal of Geophysical Research: Space Physics*, *118*, 756–764. https://doi.org/10.1029/2012JA018179